# Thermal Expansion and Response to Pressure of the Double-ReO<sub>3</sub>-type Fluorides NaM $^{V}$ F<sub>6</sub> (M = Nb, Ta)

Anthony J. Lloyd II, † Eric B. Masterson, † Samuel J. Baxter, † Jamie J. Molaison, † António M. dos Santos † and Angus P. Wilkinson \*† §

<sup>†</sup>School of Chemistry and Biochemistry and <sup>§</sup>School of Materials Science and Engineering, Georgia Institute of Technology, Atlanta, Georgia 30332, United States. <sup>‡</sup>Neutron Scattering Division, Oak Ridge National Laboratory, Oak Ridge, Tennessee 37831, United States

**ABSTRACT:** Several II-IV double-ReO<sub>3</sub>-type (DROT) fluorides are known to exhibit strong negative thermal expansion (NTE) over a wide temperature range while retaining a cubic structure down to 120 K or lower. CaZrF<sub>6</sub>, CaNbF<sub>6</sub>, CaTiF<sub>6</sub>, and MgZrF<sub>6</sub>, embody these properties. In contrast to the behavior of these II-IV materials, the I-V DROT material, NaSbF<sub>6</sub>, has been reported to display a phase transition from rhombohedral to cubic above 300 K and positive thermal expansion both above and below the transition. In this work, NaNbF<sub>6</sub> and NaTaF<sub>6</sub> are shown to undergo first-order cubic-to-rhombohedral transitions on cooling to ~130 K. Above this transition, NaNbF<sub>6</sub> shows modest NTE between 160 and 250 K, whereas NaTaF<sub>6</sub> exhibits near-zero thermal expansion over the range 210 – 270 K. These I-V systems are elastically softer than their II-IV counterparts, with a zero pressure bulk modulus,  $K_0$ , of 14.6(8) GPa and first derivative of the bulk modulus with respect to pressure,  $K'_0$ , of -18(3) for cubic NaNbF<sub>6</sub>, and  $K_0$  = 14.47(3) GPa and  $K'_0$  = -21.56(7) for cubic NaTaF<sub>6</sub>. When subject to ~0.3 GPa at 300 K, both compounds exhibit a phase transition from  $Fm\overline{3}m$  to  $R\overline{3}$ . The  $R\overline{3}$  phases exhibit negative linear compressibility over a limited pressure range. A further transition with phase coexistence occurs at ~2.5 - 3.0 GPa for NaNbF<sub>6</sub> and ~4.5 GPa for NaTaF<sub>6</sub>. Compression of NaNbF<sub>6</sub> in helium at room temperature and below provides no evidence for helium penetration into the structure to form a perovskite with helium on the A-site, as was previously reported for CaZrF<sub>6</sub>.

#### 1. INTRODUCTION

ReO<sub>3</sub>-type fluorides and oxyfluorides have attracted attention over the last decade for their potential as negative or low thermal expansion materials and because their simple crystal structures make them good candidates for studies examining the mechanisms responsible for their properties. While many different families of materials (oxides, nitrides, phosphates, intermetallics, MOFs, etc.) are known to show negative thermal expansion (NTE), 1-3 ReO<sub>3</sub>-type fluorides are of particular interest as, with the correct choice of cations, optical transparency from the mid-IR out into the UV is, in principle, achievable.4 TaO<sub>2</sub>F displays close to zero thermal expansion over a wide temperature range.5 Materials such as ScF<sub>3</sub>,6 and the cation ordered double ReO<sub>3</sub>-type (DROT) compounds CaZrF<sub>6</sub>,7 and CaNbF<sub>6</sub><sup>4</sup> show strong negative thermal expansion over a very wide temperature range (> 1000 K). CaNbF<sub>6</sub> has been reported to show a greater NTE capacity, which is a larger total volume contraction on heating, than any material investigated to date.8 The unusual thermal expansion characteristics of these compounds arises from their lattice dynamics.9,10

Since the original discovery of strong NTE in ScF $_3$ ,6 many different methods for controlling the thermal expansion of ReO $_3$ -type fluorides have been considered. These include solid solution formation in simple trifluorides, $^{11\cdot15}$  insertion of species in the vacant "A-site" of the ReO $_3$ -structure, $^{16,17}$  and the preparation of cation ordered double ReO $_3$ -type (DROT) fluorides such as CaZrF $_6$ . $^{4,7,18\cdot20}$  Nearly all of the work on DROTs has focused on II-IV materials, such as Ca $^{11}$ Zr $^{1V}$ F $_6$ , with little attention paid to the possibility of low or negative thermal expansion in I-V compounds. $^{21}$ 

Symmetry-lowering phase transitions involving the cooperative octahedral tilting of framework octahedra are commonplace in simple ReO<sub>3</sub>-type and DROT fluorides<sup>6,22</sup> upon cooing and compression. From the standpoint of negative thermal expansion, these phase transitions are undesirable, as the low-symmetry phase always displays strong positive volume thermal expansion and, in cases where the phase transition is at or above room temperature, the high temperature cubic phase does not typically show notable negative thermal expansion.<sup>23</sup> The use of very electropositive cations, such as scandium in ScF<sub>3</sub> and calcium/zirconium in CaZrF<sub>6</sub> completely suppresses tilting transitions at ambient pressure in these systems and allows for strong NTE over a wide temperature range.

The phase transitions and thermal expansion of the I-V DROT NaSbF<sub>6</sub> has been recently investigated.<sup>21</sup> It displays a first-order cubic to rhombohedral  $(Fm\bar{3}m \text{ to } R\bar{3})$  phase transition on cooling between 303 and 323 K, and the cubic form has a volumetric coefficient of thermal expansion (CTE) of  $\sim +62$  ppmK<sup>-1</sup> (300 – 650 K). This large positive CTE was attributed in part to the elongation of the Na-F bond upon heating.  $^{21}$  Several other NaM $^{V}$ F $_{6}$  are also known to adopt a cubic DROT structure at room temperature.<sup>24</sup> In this paper, we explore the thermal expansion and response to compression of NaNbF6 and NaTaF6. These compositions were chosen as both niobium and tantalum are more electropositive than antimony (electronegativities of 1.23, 1.33 and 1.82 respectively), 25 suggesting that any octahedral tilting transitions in these materials would occur at lower temperature than that observed for NaSbF6 and potentially opening up a temperature window for NTE. The behavior of NaNbF<sub>6</sub> in high-pressure helium was also explored, as helium has been reported to penetrate into CaZrF<sub>6</sub>, leading to the formation of a defect perovskite with helium on the A-site.<sup>17</sup>

#### 2. EXPERIMENTAL

**2.1 Sample Preparation.** Syntheses of both NaNbF<sub>6</sub> and NaTaF<sub>6</sub> were conducted by the direct high temperature reaction of binary fluorides. For NaNbF<sub>6</sub>, stoichiometric amounts of both NaF (Aldrich, 99.99%) and NbF<sub>5</sub> (Strem, 99.5%) were mixed and ground together with mortar and pestle in a nitrogen glovebox. The starting materials for NaTaF<sub>6</sub> – NaF (Aldrich, 99.99%) and TaF<sub>5</sub> (Alfa, 99.5%) were treated similarly. Both mixtures were sealed by arc welding in nickel tubes without exposure to air. The nickel tubes were then heated to 573 K over a 2 hour period, held at this temperature for 24 hours, and slow-cooled back to room temperature over the course of 15 hours. Note that both NaNbF<sub>6</sub> and NaTaF<sub>6</sub> decompose readily on exposure to moisture and skin contact could lead to fluoride burns.

**2.2 Variable-Temperature Powder X-Ray Diffraction Measurements.** Synchrotron X-ray diffraction data were acquired using beam line 17-BM at Argonne National Laboratory's Advanced Photon Source (APS). Samples were handled in a dry nitrogen-filled glove bag. The samples were mixed and ground with silicon powder (~2:1 volume ratio), which was used as both an internal standard and to reduce the overall X-ray absorption. These mixtures were then packed into fused quartz capillary tubes, which were sealed at both ends with epoxy. During data collection, the sample temperature was varied over the range ~ 100 – 500 K, using an Oxford Cryosystems Cryostream. Data were recorded on a Perkin-Elmer amorphous silicon 2D detector. Data were collected over multiple beam times, each with slightly different wavelength. In each the X-ray energy was precisely calibrated and close to 27.4 keV

**2.3** High-Pressure Powder X-Ray Diffraction Measurements. High pressure ambient temperature synchrotron X-ray diffraction data were acquired using beam line17-BM, at Argonne National Laboratory's APS. Samples were ground and mixed with sodium chloride, which was used as an internal pressure standard, <sup>26</sup> and then loaded into a Diacell Bragg-(G) diamond anvil cell (DAC). Silicone oil (Alfa MW =  $237~{\rm g\cdot mol^{-1}}$ ) was used as a pressure-transmitting medium. All sample handling was performed in a dry nitrogen glove bag. A diaphragm attachment was used to increase the pressure from ambient to ~ 7 GPa. Data were recorded, using ~27.4 keV X-rays, on a Perkin-Elmer amorphous silicon detector.

**2.4 Variable-Temperature, High-Pressure Powder Neutron Diffraction Measurements.** Neutron diffraction data for NaNbF<sub>6</sub> were recorded at the Spallation Neutron Source (SNS), Oak Ridge National Laboratory, using the instrument SNAP. The instrument was configured with its two detector banks centered at 2θ angles of 58 and 90 degrees. The sample was ground in a nitrogen glove box and loaded into an aluminum foil packet, which was placed in an autofrettaged aluminum gas pressure cell (maximum working pressure ~0.48 GPa).<sup>27</sup> A radial collimator was mounted directly on the pressure cell body to suppress scattering from the cell body.<sup>27</sup> The pressure cell was mounted in a top loading helium refrigerator. Helium was used as the pressure medium for most experiments, but some data were taken using an argon pressure medium. The instrument was calibrated to reproduce the ambient pressure/temperature lattice constant of the material. Typically, data were recorded

for 20 minutes at each pressure/temperature combination. To minimize the time spent waiting for thermal equilibration, data were recorded on compression at constant temperature where possible.

#### 2.5 Analyses of the Powder X-Ray Diffraction Data.

The 2D X-ray diffraction data were radially integrated using GSAS II. Rietveld analyses were performed using GSAS in conjunction with EXPGUI. Ph. 30 The analyses made use of cation-ordered cubic,  $Fm\overline{3}m$ , and rhombohedral,  $R\overline{3}$ , models. In the case of the high-pressure measurements, two-phase refinements (NaNbF6 +NaCl) were conducted until the sample underwent a transition to an unknown or amorphous phase. After this occurred, single phase fits (NaCl) were performed. The unit cell volume of the internal standard (NaCl) was used, along with the Birch equation of state for NaCl, to determine the pressure. Example fits to the variable temperature X-ray data for cubic NaNbF6 and NaTaF6 are shown in Figure 1.

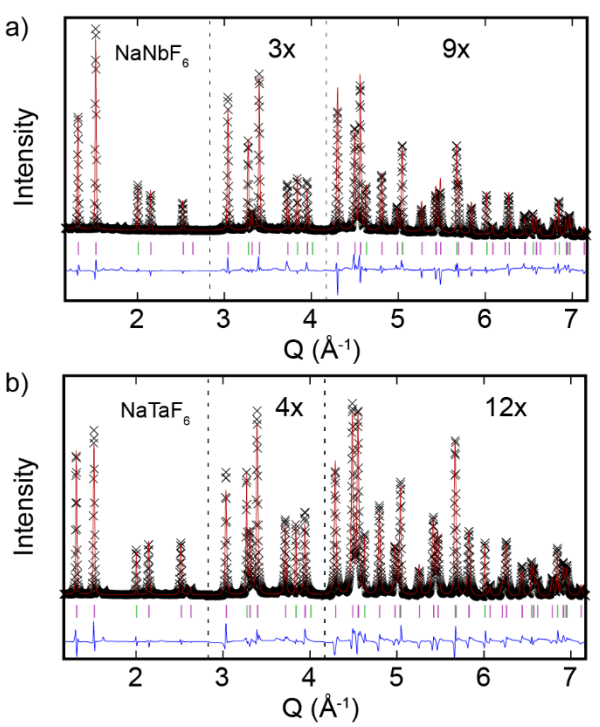


Figure 1. Rietveld fits to synchrotron diffraction data for cubic a) NaNbF<sub>6</sub> (299 K) and b) NaTaF<sub>6</sub> (299 K) at ambient pressure. The magenta and green tick marks indicate the positions of peaks from the sample and silicon standard respectively.

#### 2.6 Analyses of the Powder Neutron Diffraction Data

Data from the lower angle detector bank were used to determine, by inspection, whether the sample was predominantly cubic or rhombohedral at a particular temperature and pressure. Data from the higher angle detector bank were used in Rietveld analyses using the corresponding cubic or rhombohedral model. The analyses were performed with GSAS in conjunction with EXPGUI. <sup>29,30</sup>

#### 3. RESULTS AND DISCUSSION

### 3.1 Response of NaNbF $_6$ and NaTaF $_6$ to Temperature as Seen by X-rays

Both NaNbF<sub>6</sub> and NaTaF<sub>6</sub> undergo a phase transition at ~130 K between their ambient  $Fm\overline{3}m$  phase and the expected, low-T,  $R\overline{3}$ 

phase. This transition involves a Glazer a a type tilting of the octahedra, <sup>31</sup> leading to a reduction in the Na-F-(Nb/Ta) bond angle from  $180^{0}$  on cooling (Fig. 2a). A volumetric discontinuity at the transition and phase coexistence (Fig. 2 and Fig. S1) over a significant temperature range ( $\sim$ 120 – 130 K for NaNbF<sub>6</sub>) indicate that the transitions are first order.

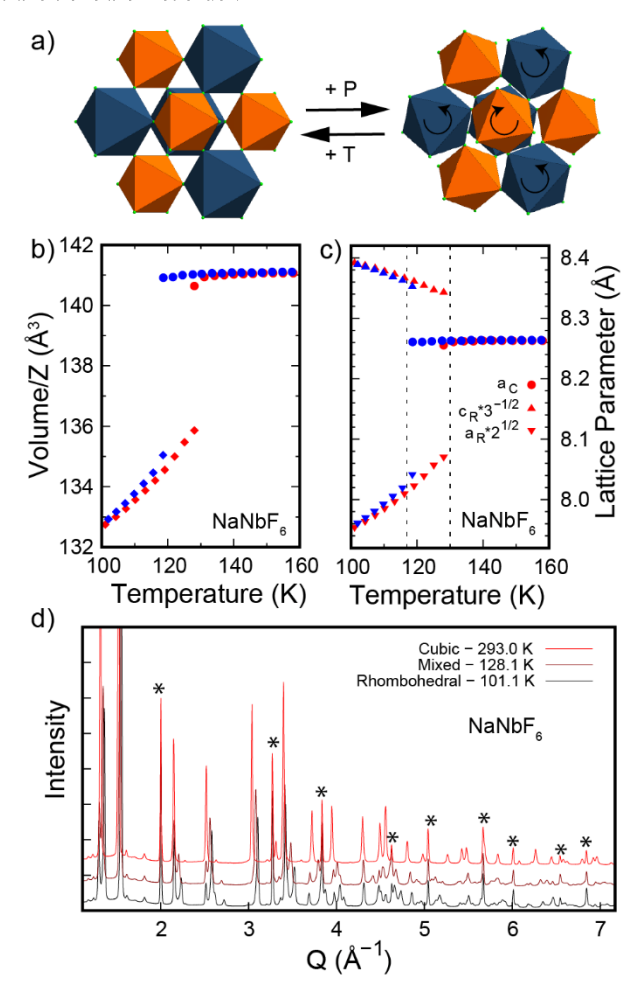


Figure 2. a) On compression or cooling, the materials undergo a phase transition where the octahedra rotate around their three-fold axes to give a rhombohedral distortion. b) Volume per formula unit versus temperature and c) lattice parameters for NaNbF6 on heating (red symbols) and cooling (blue symbols) from the X-ray diffraction data. These data indicate significant hysteresis. d) Diffraction data for NaNbF6 showing the changes associated with the phase transition and phase coexistence. The sharp peaks, marked with a \*, that are largely invariant on cooling come from the silicon internal standard.

As is typical for DROT materials, the rhombohedral form of NaNbF6 shows large volumetric positive thermal expansion (PTE),  $\sim 1000~ppmK^{-1}$ , but the cubic phase shows modest negative thermal expansion (NTE) over the temperature range  $\sim\!160$  - 250 K (Fig. 3a). NaTaF6 shows similar behavior to that of NaNbF6, but with slightly larger PTE for the rhombohedral phase,  $\sim\!1100~ppmK^{-1}$  and low positive thermal expansion ( $\alpha_1\!\sim\!1\text{-}2~ppmK^{-1}$ ) for the cubic phase in the range  $\sim\!210$  - 270 K (Fig. 3c). As expected from prior work on ReO3-type fluorides, the thermal expansion of the rhombohedral phase is highly anisotropic (Fig. 2b).  $^{4,18,19}$  The material displays very strong positive thermal expansion in the a-b plane due to a rotation

of the  $MF_6$  octahedra around their three fold axes, which opens up the Na-F-(Nb/Ta) bond angles on heating and increases the Na – (Nb/Ta) separation.

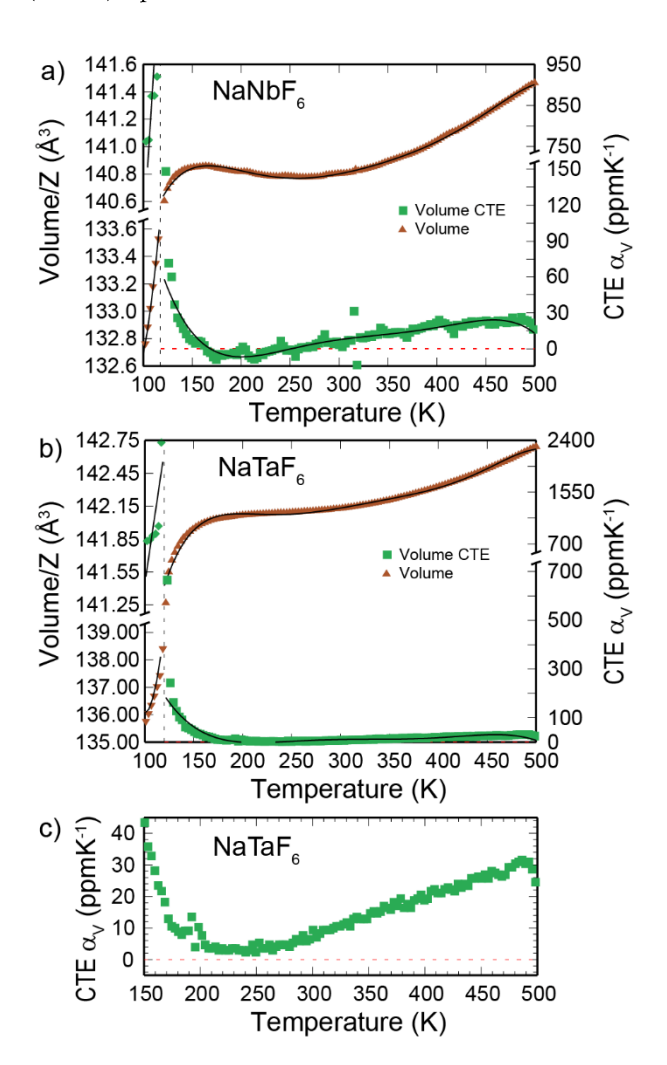


Figure 3. Unit cell volume and volumetric thermal expansion coefficients for a) NaNbF<sub>6</sub> and b) NaTaF<sub>6</sub>. c) Detail of the volumetric thermal expansion coefficient for NaTaF<sub>6</sub>. In panels a) and b) the lines drawn through the volume data are polynomial fits (2 and  $6^{th}$  order for the rhombohedral and cubic regions respectively). The CTEs were estimated point by point (the symbols) and by differentiation of the polynomial fits (lines). The "noise" in the point by point CTEs for NaNbF<sub>6</sub> arise from beam instability during the experiment. All the above were determined on cooling.

It is notable, that the expansion coefficients of both cubic NaNbF<sub>6</sub> and NaTaF<sub>6</sub> ( $\alpha_v \sim +20~ppmK^{-1}~300-500~K$  for both) are much lower than that for NaSbF<sub>6</sub> ( $\alpha_v +62~ppmK^{-1}~300-650~K$ ), <sup>21</sup> but much higher than that for Ca<sup>(II)</sup>Nb<sup>(IV)</sup>F<sub>6</sub> ( $\alpha_v \sim -32~ppmK^{-1}~300-650~K$ ). <sup>4</sup> The large positive thermal expansion of cubic NaSbF<sub>6</sub> has been attributed to an increase in Na-F distance on heating. Data in the SI for Yang et al. <sup>21</sup> indicate that the apparent (crystallographic) Na-F distance expands at  $\sim +200~ppmK^{-1}$  between 325 and 525 K and the apparent Sb-F distance contracts at  $\sim -100~ppmK^{-1}$  over the same temperature range. These changes reflect the trends in the distances between average (crystallographic) atomic positions, not true bond

length changes, which in both cases are expected to increase on heating. This behavior contrasts with that seen for NaNbF<sub>6</sub> (Fig. 4) (Na-F ~+60 ppmK<sup>-1</sup> and Nb-F ~ -60 ppmK<sup>-1</sup> over the temperature range 300-500 K), and also CaNbF<sub>6</sub> (Ca-F ~ -11 ppmK<sup>-1</sup> and Nb-F ~ -25 ppmK<sup>-1</sup> over the temperature range 100-300 K).

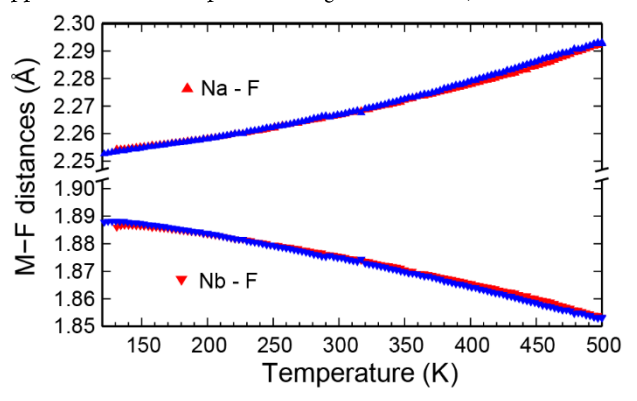


Figure 4. Variation of the apparent Na-F and Nb-F bond lengths for cubic NaNbF<sub>6</sub> with temperature. Blue triangles are the values determined on cooling and the red ones are the values determined on heating.

### 3.2 Behavior of NaNbF<sub>6</sub> and NaTaF<sub>6</sub> Upon Compression as seen by X-ray diffraction

Similar to the temperature-induced phase transitions in NaNbF<sub>6</sub> and NaTaF<sub>6</sub>, both compounds display a pressure-induced, symmetry-lowering phase transition at ~0.3 GPa and room temperature to a rhombohedral ( $R\overline{3}$ ) phase (Fig. 5). The transition pressure is higher than that for NaSbF<sub>6</sub> (~0.1 GPa),<sup>32</sup> but comparable to that for MgZrF<sub>6</sub> (0.37 GPa).<sup>4</sup> This transition is associated with cooperative tilting of the octahedra (Fig 2a). An additional phase transition, with phase coexistence is observed at ~2.5 – 3.0 GPa for NaNbF<sub>6</sub> and ~4.5 GPa for NaTaF<sub>6</sub>. Both compounds seem to adopt the same, as yet unidentified, structure at higher pressure.

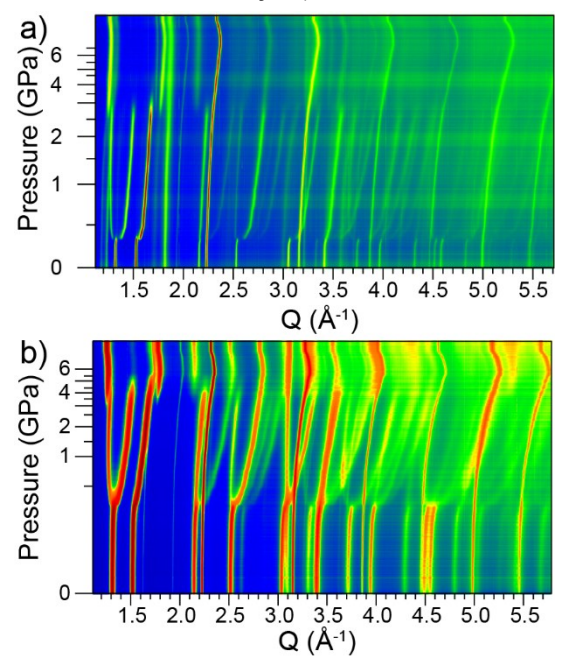


Figure 5. Powder diffraction data recorded on the compression of a) NaNbF6 and b) NaTaF6.

Fits of a third order Birch-Murnaghan equation of state (EoS), performed using EoS fit,  $^{33}$  to volume versus pressure for the cubic phase (Fig. 6), indicate that both NaNbF6 and NaTaF6 are soft (K0 14.6 and 15.5 GPa respectively) when compared to  $M^{II}M^{IV}F_6$  DROTs (K0 377 and 48.24 GPa for CaZrF6 and MgZrF6 respectively). Both also display pressure induced softening, which is typical for materials in this class and has been predicted to be a feature of NTE materials.  $^{9,34,35}$ 

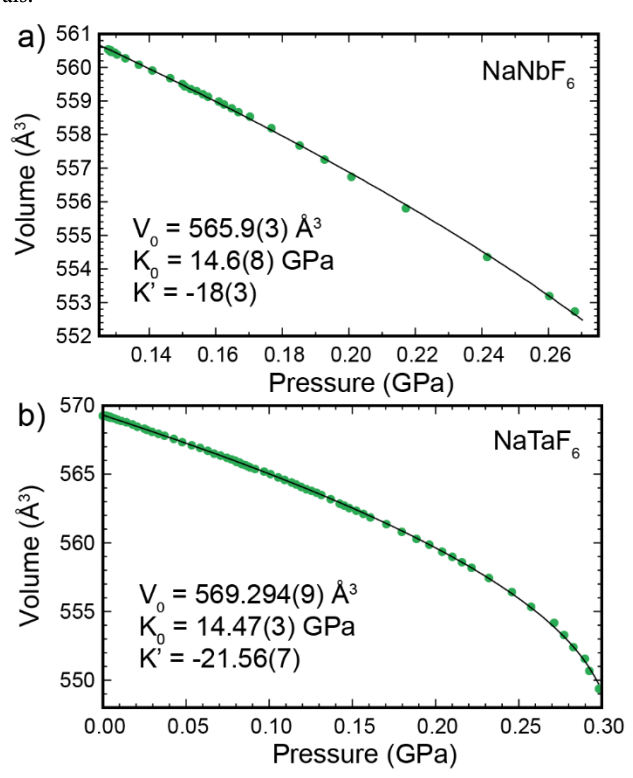


Figure 6. Volume versus pressure from the X-ray experiments for cubic a) NaNbF<sub>6</sub> and b) NaTaF<sub>6</sub> fit to a third-order Birch-Murnaghan equation of state.

The transition from the cubic to the rhombohedral phase on compression is clearly first order for NaNbF6, with phase coexistence over a significant range and a volume discontinuity (Fig.5a, Fig. 7a). However, the transition for NaTaF6 is not so clearly first order (Fig. 5b and Fig. S3). The rhombohedral phase undergoes strongly anisotropic compression. In the a-b plane, the materials are very soft, as rotation of the octahedra around a 3-fold axis leads to reduction in the Na-F-(Nb/Ta) bond angles. However, parallel to the crystallographic c-axis, the materials display negative linear compressibility (Fig. 7b) immediately after the phase transition up to ~1 GPa. Similar behavior has been observed in MF3 phases³6 and related materials such as CaTiF6¹9 and MnNbF6,¹8 and it has been associated with a distortion of the MF6 octahedra as they rotate.

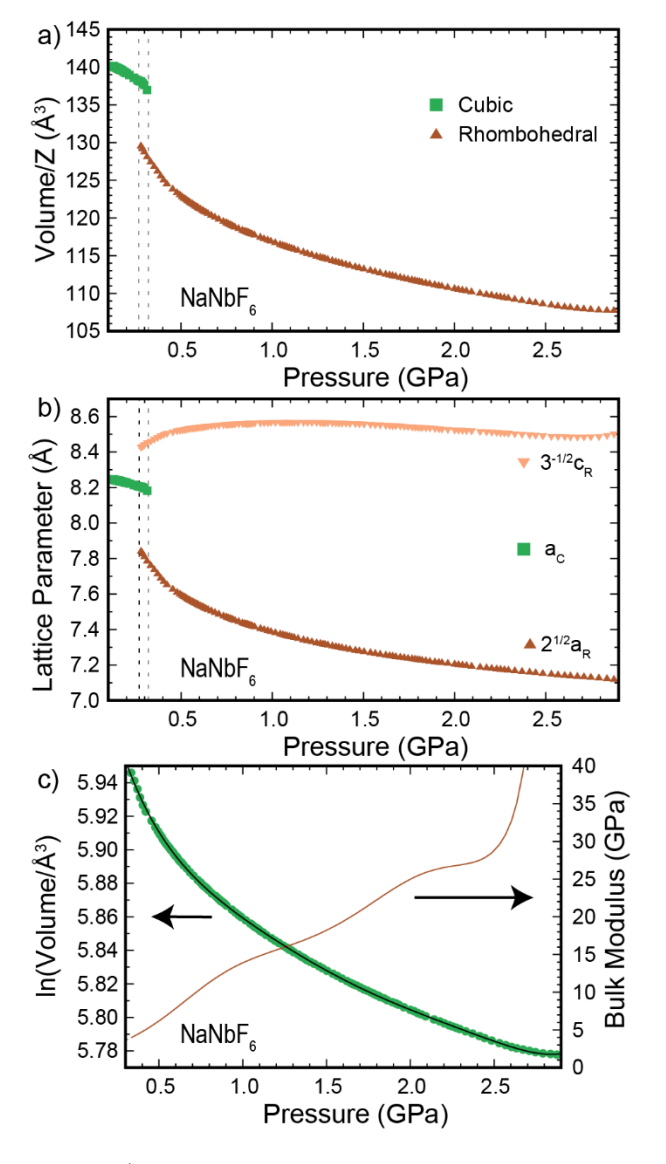


Figure 7. a) Volume versus pressure for cubic and rhombohedral NaNbF<sub>6</sub>, b) lattice constants versus pressure for NaNbF<sub>6</sub> and c) a sixth order polynomial fit to log volume versus pressure for rhombohedral NaNbF<sub>6</sub> along with the phase's bulk modulus obtained by differentiating the polynomial. All the underlying data were obtained using X-ray diffraction.

For an ideal ReO $_3$ -type material, rotation of the octahedra around their three-fold axes is limited. After a 30 $^0$  rotation away from the cubic form, the anions in the structure become close packed, with M-X-M angles of 131.8 $^0$ , which, when projected onto the a-b plane, corresponds to 120 $^0$ . The evolution of the projection of the Na-F-Ta/Nb bond angles in NaNbF $_6$  and NaTaF $_6$  onto the a-b plane with pressure are shown in Figure 8. These angle estimates make use of the fluorine coordinates obtained from Rietveld analyses of the high pressure X-ray data and may have significant errors associated with them due to the limited Q range and quality of the high pressure data. For NaNbF $_6$ , the angle evolves from ~160 to 128 $^0$  between the cubic to rhombohedral phase transition at ~0.3 GPa and the second transition at ~3.0 GPa. The starting angle of 160 $^0$ , rather than 180 $^0$ , is a consequence of the cubic to rhombohedral phase transition being first order. The origin of the small hump in Fig. 8a centered at

 $\sim$ 0.6 GPa is unknown, but it is likely an artifact. For NaTaF<sub>6</sub>, the projection of the Na-F-Ta angle evolves from close to 180 to  $\sim$ 120°, as the cubic to rhombohedral first transition is less obviously first order than that in NaNbF<sub>6</sub>. Once the projection of this angle reaches  $\sim$ 120°, and the anions are effectively close packed, further densification on compression can't be achieved by simply rotating incompressible octahedra. Jorgsensen has proposed that some further compression can be achieved in simple MF<sub>3</sub> structures by adopting a "super-dense" sphere packing where triangles of anions, associated with octahedral faces, are compressed.<sup>36</sup> It should be noted that for both NaNbF<sub>6</sub> and NaTaF<sub>6</sub>, a phase transition to a different structure is observed at close to the point where anion closest packing would be achieved. This likely involves a change in coordination number for the ions in the material.

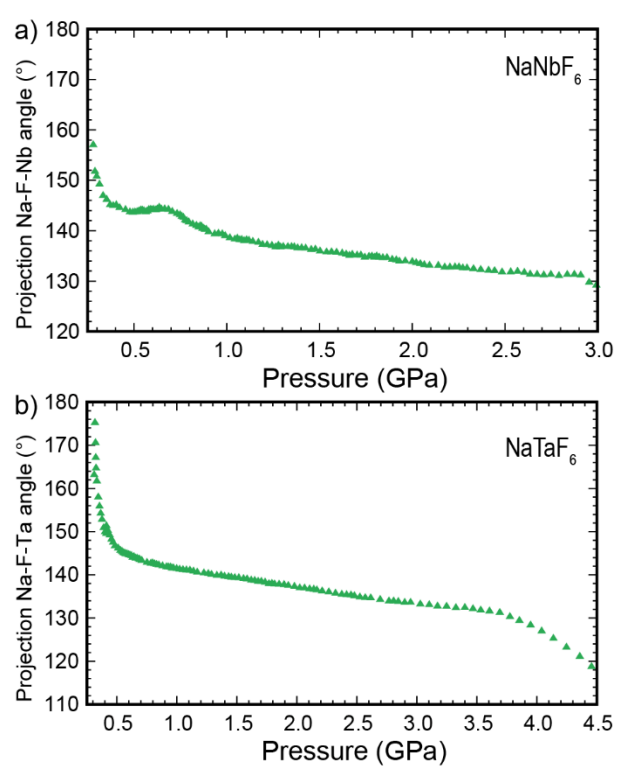


Figure 8. Projection of the Na-F-(Nb/Ta) bond angle onto the crystallographic a-b plane for a) NaNbF<sub>6</sub> and b) NaTaF<sub>6</sub>. In the cubic-phase, this angle is  $180^{\circ}$  and anion closest packing is achieved for an ideal structure at  $120^{\circ}$ .

The stiffness of the rhombohedral phases increases on compression. As estimates of volume versus pressure for the rhombohedral phase could not be satisfactorily fit using an equation of state, a polynomial fit to log volume versus pressure was used to estimate the pressure dependence of the bulk modulus (Fig. 7c and Fig S3). Immediately above the phase transition, the material's bulk moduli are extremely low ( $\sim$ 5 GPa for NaNbF6, Fig 7c). However, they rapidly stiffen on compression, presumably because the volume reduction, associated with a reduction in the Na-F-(Nb/Ta) bond angles, brings the ions closer together, leading to increased repulsion.

## 3.3 Behavior of $NaNbF_6$ and $NaTaF_6$ Upon Compression and Cooling as seen by Neutron Diffraction

It has previously been reported that helium can be inserted into Ca-ZrF<sub>6</sub> at high pressures, and temperatures above  $\sim$ 200 K, to form a

defect perovskite with helium on the A-site,  $[He_{2x}\Box_x][CaZr]F_6$ . The insertion of helium into the structure was observed to change its phase behavior on compression. As the room temperature lattice constant for NaNbF<sub>6</sub> (8.26 Å) is only 2.5 % smaller than that of CaZrF<sub>6</sub> (8.47 Å), neutron diffraction studies of NaNbF<sub>6</sub> in high pressure helium were conducted to investigate the potential insertion of helium into this framework, along with the low temperature high pressure behavior of this material.

Initial room temperature (~295 K) neutron measurements using an argon gas medium showed a phase transition at ~0.3 GPa. A Burch-Murnaghan EoS fit to volume versus pressure for the cubic phase (Fig. S4) gave estimates for  $K_0$  and  $K'_0$  of 12.5(6) GPa and -11(4) respectively, in reasonable agreement with those estimated from the room temperature X-ray diffraction data,14.6(8) GPa and -18(3) respectively (Fig. 6a). After switching to a helium gas medium, a cubic to rhombohedral phase transition was still observed at close to 0.3 GPa on compression at room temperature (Fig. 9). This strongly suggests that helium is not inserted into the structure on the time scale of these measurements, as the presence of helium on the material's A-site would likely change its phase behavior. The time scale for helium insertion into CaZrF6 is reported to be several minutes at room temperature.<sup>17</sup> As the lattice constant for cubic NaNbF<sub>6</sub> is smaller than that for CaZrF<sub>6</sub>, the time dependence of the lattice constant for NaNbF6 at room temperature, as it was exposed to helium at successively higher pressures, was examined over a time interval of ~6 hours (see Fig. S5). There was no systematic time dependence, beyond what could be reasonably attributed to some leakage from the pressure vessel, again suggesting that helium does not penetrate into NaNbF6 at room temperature. While sitting at 0.325 GPa and 295 K the sample was observed to transform, with no obvious phase coexistence, from cubic to rhombohedral symmetry. An EoS fit to volume versus pressure, using the data from the time dependent measurements (Fig. S6), gave estimates for K<sub>0</sub> and K'<sub>0</sub> of 8.8(4) GPa and 44(5), somewhat different from the values obtained from the earlier measurements in argon. However, this difference is not great given the scatter in the data, and it is inconsistent with the stiffening that is expected on the insertion of helium. An examination of the phase behavior in helium (Fig. 9) over the pressure and temperature range 0 - 0.45 GPa and 80 - 295 K is fully consistent with that observed by X-ray diffraction, supporting the proposal that helium is not interested into NaNbF6 under the conditions explored. The cubic to rhombohedral phase transition is first order with considerable hysteresis on compression and decompression (Fig. 9b) at room temperature.

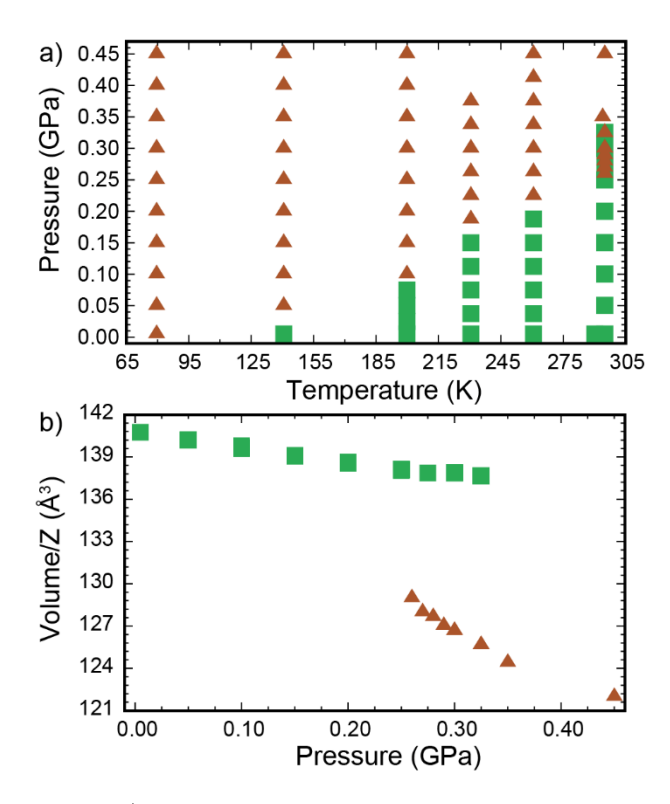


Figure 9. a) Phase behavior of NaNbF6 as seen by neutron diffraction using a helium pressure medium. Green squares indicate cubic and brown triangles indicate rhombohedral. b) Hysteresis in the phase transition at 295 K. The green points in (b) were recorded on compression, whereas some of the brown points were recorded on decompression of a rhombohedral sample.

Data recorded for the cubic phase on compression at different temperatures (Fig. 10a) gave bulk modulus estimates (Fig. S7) that were consistent with no helium penetrating into the structure. Volume versus pressure, for the rhombohedral phase at different temperatures, is also shown in Fig. 10a. As expected, the rhombohedral phase shows positive thermal expansion over the pressure range investigated, and the volume coefficient of thermal expansion decreases in magnitude on compression, as can be seen most readily by looking at the decrease in difference between V/Z at 200 and 80 K as the pressure goes up. However, the crystallographic c-axis for the rhombohedral phase displays negative thermal expansion over the full pressure range studied (Fig. 10b). The positive volume thermal expansion of the rhombohedral phase arises from the response of the material in the a-b plane.

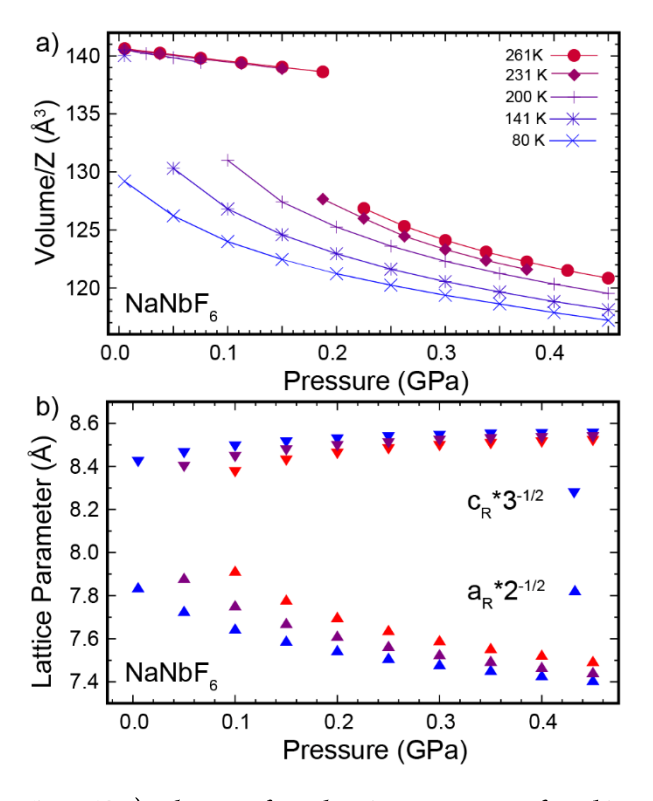


Figure 10. a) Volume per formula unit versus pressure for cubic and rhombohedral NaNbF $_6$  at different temperatures. b) Lattice constants for rhombohedral NaNbF $_6$  at 80 (blue), 141 (purple) and 200 K (red). Data were collected on increasing the pressure.

The pressure dependence of thermal expansion is intimately related to the temperature dependence of a material's isothermal bulk modulus (equation 1).<sup>37</sup>

$$\left(\frac{\partial \alpha_V}{\partial P}\right)_T = \frac{1}{K_T^2} \left(\frac{\partial K_T}{\partial T}\right)_P (1)$$

The observed decrease in  $\alpha_V$  on compression requires that the material also softens on heating, as the bulk modulus is positive. Attempts to quantify the bulk modulus for the rhombohedral phase at different temperatures, by fitting a Birch-Murnaghan equation of state were unsuccessful, as this function could not adequately describe the volume pressure data. However, a Vinet equation of state provided a reasonable fit to the data at 80 and 141 K (Fig. 11 and Fig. S8). The estimated bulk moduli at zero pressure were very small, 1.34(8) and 0.35(6) GPa respectively, but consistent with the expected softening on heating.

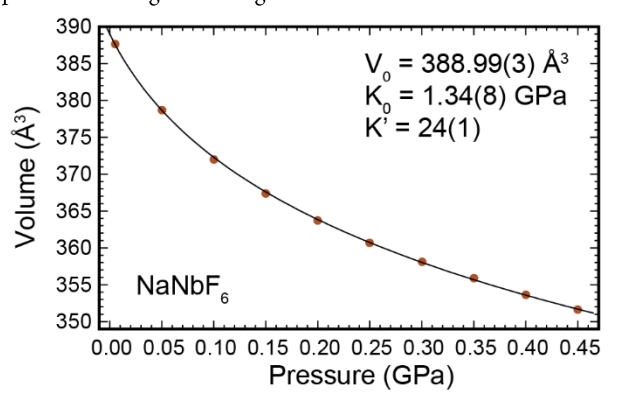


Figure 11. Volume versus pressure at 80 K for rhombohedral  $NaNbF_6$  along with a fit to a Vinet equation of state.

#### 3.4 A Comparison of NaNbF6 and NaTaF6 with NaSbF6

Yang et al.<sup>21</sup> reported that NaSbF<sub>6</sub> undergoes a cubic to rhombohedral transition on cooling below room temperature and that the cubic high temperature phase shows strong positive thermal expansion. Sowa reported that on compressing cubic NaSbF<sub>6</sub> at room temperature a  $Fm\overline{3}m$  to  $R\overline{3}$  phase transition occurred at < 0.1 GPa.<sup>32</sup> The low phase transition pressure precluded characterization of the cubic phase. No other transitions were observed on compression of NaSbF<sub>6</sub> up to ~5.6 GPa.

NaNbF<sub>6</sub> and NaTaF<sub>6</sub> both display a cubic to rhombohedral phase transition at much lower temperature (~130 K) than NaSbF $_6$ (323 K).21 The suppression of this phase transition opens up a temperature window where modest NTE (NaNbF<sub>6</sub> 160 - 250 K) or very low PTE (NaTaF<sub>6</sub> 210-270 K) are displayed. It is also associated with a much lower expansion coefficient at higher temperatures. The occurrence of NTE mirrors the behavior of many II-IV DROT materials that undergo a rhombohedral-to-cubic phase transition below 150 K. NaNbF6 and NaTaF6 are the first I-V DROTs to show low or negative thermal expansion. The replacement of antimony by the more electropositive elements niobium and tantalum also increases the pressure at which a cubic to rhombohedral transition is seen on compression from ~0.1 GPa to ~0.3 GPa enabling the characterization of the cubic phase on compression. Cubic NaNbF6 and NaTaF6 are both elastically soft and display strong pressure induced softening prior to their cubic to rhombohedral phase transitions. Unlike NaSbF<sub>6</sub>, NaNbF<sub>6</sub> and NaTaF<sub>6</sub> both display an additional phase transition on compression.

The observed changes in thermal expansion and phase transition temperature/pressure on replacing antimony by niobium, or tantalum, are intimately linked to one another, as they all depend up on the lattice dynamics of the materials. The replacement of antimony by another element changes the interatomic potentials, and this changes the phonon dispersion curves for the materials, and how they respond to both volume reduction and temperature change, so any change in chemistry will both change the thermal expansion and phase transitions.

#### 4. CONCLUSIONS

The replacement of antimony by the larger and less electronegative elements niobium or tantalum stabilized a cubic DROT structure to lower temperature and higher pressure. This opened up a temperature window for negative thermal expansion in cubic NaNbF<sub>6</sub>. Although the lattice constant of NaNbF<sub>6</sub> is only 2.5% less than that of CaZrF<sub>6</sub>, experiments in high pressure helium at room temperature and below provided no evidence for the penetration of helium into the structure to form a perovskite with helium on the A-site, of the type previously reported for CaZrF<sub>6</sub>. While the CTEs for NaTaF<sub>6</sub> and NaNbF<sub>6</sub> around room temperature are low, the great sensitivity of these materials to moisture likely precludes application.

#### **ASSOCIATED CONTENT:**

**Supporting Information.** Example Rietveld fits. Lattice constants versus temperature and pressure. Equation of state fits. Crystallographic information.

#### **AUTHOR INFORMATION**

#### **Corresponding Author**

\*E-mail: angus.wilkinson@chemistry.gatech.edu.

#### **ORCID**

Angus P. Wilkinson: 0000-0003-2904-400X

#### **ACKNOWLEDGMENT**

We are grateful for experimental assistance from the staff of beamline 17-BM at the Advanced Photon Source and both the sample environment team, and instrument staff of the SNAP beam line, at the Spallation Neutron Source. The work at Georgia Tech was partially financially supported under NSF DMR-1607316 and NSF DMR-2002739. The research made use of the Advanced Photon Source, a U.S. Department of Energy (DOE) Office of Science User Facility operated for the DOE Office of Science by Argonne National Laboratory under Contract No. DE-AC02-06CH11357. A portion of this research used resources at the Spallation Neutron Source, a DOE Office of Science User Facility operated by the Oak Ridge National Laboratory.

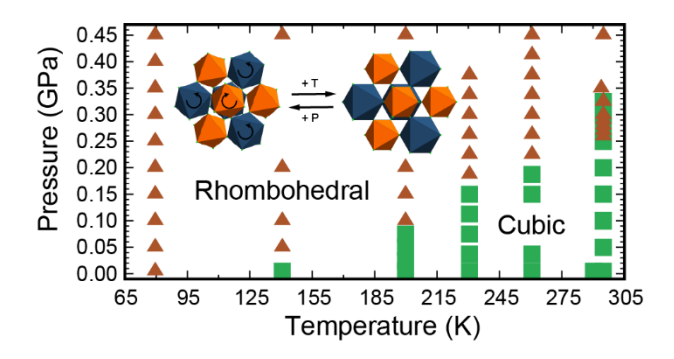
#### **REFERENCES**

- (1) Attfield, J. P. Mechanisms and Materials for NTE. Front. Chem. (Lausanne, Switz.) **2018**, 6, 6.
- (2) Chen, J.; Hu, L.; Deng, J.; Xing, X. Negative Thermal Expansion in Functional Materials: Controllable Thermal Expansion by Chemical Modifications. *Chem. Soc. Rev.* **2015**, *44*, 3522-3567.
- (3) Takenaka, K. Progress of Research in Negative Thermal Expansion Materials: Paradigm Shift in the Control of Thermal Expansion. *Front. Chem. (Lausanne, Switz.)* **2018**, *6*.
- (4) Hester, B. R.; Hancock, J. C.; Lapidus, S. H.; Wilkinson, A. P. Composition, Response to Pressure, and Negative Thermal Expansion in  $M^{11}B^{1V}F_6$  (M = Ca, Mg; B = Zr, Nb). *Chem. Mater.* **2017**, 29, 823-831.
- (5) Tao, J. Z.; Sleight, A. W. Very Low Thermal Expansion in TaO<sub>2</sub>F. *J. Solid State Chem.* **2003**, *173*, 45-48.
- (6) Greve, B. K.; Martin, K. L.; Lee, P. L.; Chupas, P. J.; Chapman, K. W.; Wilkinson, A. P. Pronounced Negative Thermal Expansion from a Simple Structure: Cubic ScF<sub>3</sub>, *J. Am. Chem. Soc.* **2010**, *132*, 15496-15498.
- (7) Hancock, J. C.; Chapman, K. W.; Halder, G. J.; Morelock, C. R.; Kaplan, B. S.; Gallington, L. C.; Bongiorno, A.; Han, C.; Zhou, S.; Wilkinson, A. P. Large Negative Thermal Expansion and Anomalous Behavior on Compression in Cubic ReO<sub>3</sub>-type A<sup>II</sup>B<sup>IV</sup>F<sub>6</sub>: CaZrF<sub>6</sub> and CaHfF<sub>6</sub> *Chem. Mater.* **2015**, 27, 3912-3918.
- (8) Coates, C. S.; Goodwin, A. L. How to Quantify Isotropic Negative Thermal Expansion: Magnitude, Range, or Both? *Mater. Horizons* **2019**, *6*, 211-218.
- (9) Dove, M. T.; Fang, H. Negative Thermal Expansion and Associated Anomalous Physical Properties: Review of the Lattice Dynamics Theoretical Foundation. *Rep. Prog. Phys.* **2016**, *79*, 066503.
- (10) Mittal, R.; Gupta, M. K.; Chaplot, S. L. Phonons and Anomalous Thermal Expansion Behaviour in Crystalline Solids. *Prog. Mater. Sci.* **2018**, 92, 360-445.
- (11) Morelock, C. R.; Greve, B. K.; Gallington, L. C.; Chapman, K. W.; Wilkinson, A. P. Negative Thermal Expansion and Compressibility of Sc<sub>1-x</sub>Y<sub>x</sub>F<sub>3</sub> (x < 0.25). *J. Appl. Phys.* **2013**, *114*, 213501.
- (12) Morelock, C. R.; Gallington, L. C.; Wilkinson, A. P. Evolution of Negative Thermal Expansion and Phase Transitions in Sc<sub>1-x</sub>Ti<sub>x</sub>F<sub>3</sub>. *Chem. Mater.* **2014**, 26, 1936-1940.
- (13) Morelock, C. R.; Gallington, L. C.; Wilkinson, A. P. Solid Solubility, Phase Transitions, Thermal Expansion, and Compressibility in Sc<sub>1-x</sub>Al<sub>x</sub>F<sub>3</sub>. *J. Solid State Chem.* **2015**, 222, 96-102.
- (14) Qin, F.; Chen, J.; Aydemir, U.; Sanson, A.; Wang, L.; Pan, Z.; Xu, J.; Sun, C.; Ren, Y.; Deng, J.; Yu, R.; Hu, L.; Snyder, G. J.; Xing, X. Isotropic

- Zero Thermal Expansion and Local Vibrational Dynamics in  $(Sc,Fe)F_3$ . *Inorg. Chem.* **2017**, *56*, 10840-10843.
- (15) Han, F.; Chen, J.; Hu, L.; Ren, Y.; Rong, Y. C.; Pan, Z.; Deng, J. X.; Xing, X. R. The Distortion-Adjusted Change of Thermal Expansion Behavior of Cubic Magnetic Semiconductor  $(Sc_{1-x}M_x)F_3$  (M = Al, Fe). *J. Am. Ceram. Soc.* **2016**, 99, 2886-2888.
- (16) Chen, J.; Gao, Q.; Sanson, A.; Jiang, X.; Huang, Q.; Carnera, A.; Rodriguez, C. G.; Olivi, L.; Wang, L.; Hu, L.; Lin, K.; Ren, Y.; Lin, Z.; Wang, C.; Gu, L.; Deng, J.; Attfield, J. P.; Xing, X. Tunable Thermal Expansion in Framework Materials through Redox Intercalation. *Nat. Commun.* **2017**, *8*, 14441.
- (17) Hester, B. R.; dos Santos, A. M.; Molaison, J. J.; Hancock, J. C.; Wilkinson, A. P. Synthesis of Defect Perovskites (He<sub>2-x</sub>¬<sub>x</sub>)(CaZr)F<sub>6</sub> by Inserting Helium into the Negative Thermal Expansion Material CaZrF<sub>6</sub>. *J. Am. Chem. Soc.* **2017**, *139*, 13284-13287.
- (18) Hester, B. R.; Wilkinson, A. P. Effects of Composition on Crystal Structure, Thermal Expansion, and Response to Pressure in ReO<sub>3</sub>-type MNbF<sub>6</sub> (M= Mn and Zn). *J. Solid State Chem.* **2019**, 269, 428-433.
- (19) Hester, B. R.; Wilkinson, A. P. Negative Thermal Expansion, Response to Pressure and Phase Transitions in CaTiF<sub>6</sub>. *Inorg. Chem.* **2018**, 57, 11275-11281.
- (20) Hu, L.; Chen, J.; Xu, J.; Wang, N.; Han, F.; Ren, Y.; Pan, Z.; Rong, Y.; Huang, R.; Deng, J.; Li, L.; Xing, X. Atomic Linkage Flexibility Tuned Isotropic Negative, Zero, and Positive Thermal Expansion in MZrF<sub>6</sub> (M = Ca, Mn, Fe, Co, Ni, and Zn). *J. Am. Chem. Soc.* **2016**, *138*, 14530-14533.
- (21) Yang, C.; Qu, B. Y.; Pan, S. S.; Zhang, L.; Zhang, R. R.; Tong, P.; Xiao, R. C.; Lin, J. C.; Guo, X. G.; Zhang, K.; Tong, H. Y.; Lu, W. J.; Wu, Y.; Lin, S.; Song, W. H.; Sun, Y. P. Large Positive Thermal Expansion and Small Band Gap in Double-ReO<sub>3</sub>-Type Compound NaSbF<sub>6</sub>. *Inorg. Chem.* **2017**, *56*, 4990-4995.
- (22) Reinen, D.; Steffens, F. Structure and Bonding in Transition-Metal Fluorides  $M^{II}Me^{IV}F_6$  .A. Phase-Transitions. Z. Anorg. Allg. Chem. 1978, 441, 63-82.
- (23) Morelock, C. R.; Hancock, J. C.; Wilkinson, A. P. Thermal Expansion and Phase Transitions of α-AlF<sub>3</sub>. *J. Solid State Chem.* **2014**, 219, 143-147.
- (24) Kemmitt, R. D. W.; Russell, D. R.; Sharp, D. W. A. 844. The Structural Chemistry of Complex Fluorides of General Formula A<sup>1</sup>B<sup>1</sup>F<sub>6</sub>. *J. Chem. Soc.* **1963**, 4408-4413.
- (25) Little, E. J.; Jones, M. M. A complete table of electronegativities. *J. Chem. Ed.* **1960**, *37*, 231.
- (26) Birch, F. Equation of State and Thermodynamic Parameters of Sodium Chloride to 300 kbar in the High-Temperature Domain. *J. Geophys. Res. B* **1986**, *91*, 4949-4954.
- (27) dos Santos, A. M.; Molaison, J. J.; Haberl, B.; Krishna, L.; Page, K.; Loguillo, M.; Wang, X. P. The High Pressure Gas Capabilities at Oak Ridge National Laboratory's Neutron Facilities. *Rev. Sci. Instrum.* **2018**, *89*, 8.
- (28) Toby, B. H.; Von Dreele, R. B. GSAS-II: The Genesis of a Modern Open-Source All Purpose Crystallography Software Package. *J. Appl. Crystallogr.* **2013**, *46*, 544-549.
- (29) Toby, B. H. EXPGUI, a Graphical User Interface for GSAS. *J. Appl. Crystallogr.* **2001**, 34, 210-213.
- (30) Larson, A. C.; Von Dreele, R. B.: GSAS General Structure Analysis System; Report LA-UR-86-748: Los Alamos Laboratory, 1987.
- (31) Glazer, A. M. Classification of Tilted Octahedra in Perovskites. *Acta Crystallogr.* **1972**, *B28*, 3384-3392.
- (32) Sowa, H. Pressure-induced Fm-3m to R-3 Phase Transition in NaSbF<sub>6</sub>. Acta Crystallogr. Sect. B: Struct. Sci. **1997**, 53, 25-31.
- (33) Angel, R. J.; Gonzalez-Platas, J.; Alvaro, M. EosFit7c and a Fortran Module (Library) for Equation of State Calculations. *Z. Kristallogr.* **2014**, 229, 405-419.
- (34) Fang, H.; Dove, M. T.; Phillips, A. E. Common Origin of Negative Thermal Expansion and other Exotic Properties in Ceramic and Hybrid Materials. *Phys. Rev. B* **2014**, *89*, 214103.

- (35) Fang, H.; Dove, M. T. A Phenomenological Expression to Describe the Temperature Dependence of Pressure-Induced Softening in Negative Thermal Expansion Materials. *J. Phys. Condens. Matter* **2014**, 26, 115402.
- (36) Jorgensen, J. E.; Olsen, J. S.; Gerward, L. Compression mechanism of GaF3 and FeF3: a high-pressure X-ray diffraction study. *High Pressure Res.* **2010**, 30, 634-642.
- (37) Anderson, O. L.: Equations of State of Solids for Geophysics and Ceramic Science; Oxford University Press: Oxford, 1995.

### For Table of Contents Only



NaNbF $_6$  and NaTaF $_6$  undergo a phase transition on cooling below ~130 K. NaNbF $_6$  shows modest negative thermal expansion in the range 160 -250 K and NaTaF $_6$  shows low positive thermal expansion between 210 and 270 K. On compression at 295 K to ~0.3 GPa, the same transition occurs. Unlike CaZrF $_6$ , on compressing NaNbF $_6$  in helium, there were no signs that it penetrated the structure to form a perovskite with helium on the A-site.